AFOSR-TR-97

0277

REPORT DOCUMENTATION PAGE

1. AGENCY USE ONLY (Leave blank)	2. REPORT DATE	3. REPORT TYPE AND DATES COVERED
	April 22, 1997	FINAL REPORT 2/1/94 - 1/31/97

4. TITLE AND SUBTITLE
(U) "Nonlinear Optical Spectroscopy of Multicomponent Droplets AND Two- and Three-Dimensional Measurements in Flames"

5. FUNDING NUMBERS
PE - 61102F
PR - 2308
SA - CS
G - F49620-94-1-0135

6. AUTHOR(S)
Richard K. Chang and Marshall B. Long
(Co-Principal Investigators)

7. PERFORMING ORGANIZATION NAME(S) AND ADDRESS(ES)
Yale University
Dept. of Applied Physics
P.O. Box 208284
New Haven, CT 06520-8284

8. PERFORMING ORGANIZATION REPORT NUMBER

9. SPONSORING/MONITORING AGENCY NAME(S) AND ADDRESS(ES)
AFOSR/NA
110 Duncan Avenue, Suite B115
Bolling AFB DC 20332-0001

10. SPONSORING/MONITORING AGENCY REPORT NUMBER

11. SUPPLEMENTARY NOTES

12a. DISTRIBUTION/AVAILABILITY STATEMENT
Approved for public release; distribution is unlimited

12b. DISTRIBUTION CODE

13. ABSTRACT (Maximum 200 words)

Significant progress has been made in the following two research areas: **I.** Nonlinear spectroscopy of micrometer-sized multicomponent droplets; and **II.** Two- and three-dimensional scalar and velocity mapping.

I. Optical diagnostics that have the potential of providing information on chemical species and temperature of multicomponent liquid droplets have been developed. A brief summary of the research accomplishments in the following three areas: (1) droplet temperature determination with thermochromic dyes; (2) enhancement of stimulated Raman scattering from droplets for identifying chemical species; and (3) modification of droplet lasing characteristics by injection seeding and Q-switching.

II. Progress has been made in developing and applying a technique for obtaining mixture fraction and scalar dissipation in a variety of turbulent nonpremixed flames. The data from these experiments are of use for modeling these complex systems. In premixed flames, simultaneous velocity/scalar images were obtained, along with full three-dimensional gradient and OH information.

14. SUBJECT TERMS	15. NUMBER OF PAGES
Laser diagnostics, mixture fraction, Raman scattering, Particle Image Velocimetry, premixed flames, turbulent combustion, droplets, thermochromic additive, minor species, nonlinear optical diagnostics	22
	16. PRICE CODE

17. SECURITY CLASSIFICATION OF REPORT	18. SECURITY CLASSIFICATION OF THIS PAGE	19. SECURITY CLASSIFICATION OF ABSTRACT	20. LIMITATION OF ABSTRACT
Unclassified	Unclassified	Unclassified	UL

FINAL REPORT

to the

Air Force Office of Scientific Research

Nonlinear Spectroscopy of Multicomponent Droplets

and

Two- and Three-Dimensional Measurements in Flames

AFOSR Grant No. G-F49620-94-1-0135

February 1, 1994 - January 31, 1997

Richard K. Chang and Marshall B. Long

(Co-Principal Investigators)

Yale University

New Haven, Connecticut 06520-8284

March 31, 1997

CONTENTS

INTRODUCTION

During the three years of AFOSR support, significant progress has been made in the following two research areas: (1) Nonlinear spectroscopy of micrometer-sized multicomponent droplets; and (2) Two- and three-dimensional scalar and velocity mapping. Specific details of our accomplishments regarding the use of nonlinear optical spectroscopy to characterize droplets and multidimensional diagnostics in flames can be found in the publications resulting from the research (See list starting on page 15). All these papers have been submitted to AFOSR in both preprint and reprint form.

RESEARCH ACCOMPLISHMENTS

I. Nonlinear Spectroscopy of Droplets

(a) Temperature Determination

During the three year AFSOR grant period, the one new finding is the observation that the wavelength where the fluorescent-lasing transition occur shifts with temperature, when the droplet contains an appropriate mixture of lasing dye and thermochromic absorber. The latter is an absorber (within specific wavelength region) that has a temperature dependent absorption coefficient, $\alpha_{abs}(\lambda,T)$. By calibrating the wavelength of the fluorescent-lasing transition with temperature, the droplet temperature can, in principle be deduced. In order for the droplet to lase, the optical cavity modes of the droplet must provide the needed optical feedback. Because these optical cavity modes of a spherical droplet are localized within an outer band ($a/m(\omega) < r < a$, where $m(\omega)$ is the index of refraction of the liquid), the temperature which we deduce with this technique is from the outer band of the droplet.

To achieve lasing, the round-trip gain must overcome the total round-trip loss. The condition for lasing at any wavelength, λ, can be written as:

$$n_1\sigma_e(\lambda) \geq \alpha_{leakage}(\lambda) + \alpha_{abs}(\lambda, T) + n_0\sigma_a(\lambda), \qquad (1)$$

where $\sigma_e(\lambda)$ and $\sigma_a(\lambda)$ are the stimulated emission and absorption cross-section (cm^2) of the fluorescent dye. The total number of fluorescent dye molecules per unit volume is $n_T = n_0 + n_1$, where n_1 is the number density of molecules in the first excited electronic single state and n_0 is the number density of molecules in the ground electronic single state. The radiation leakage loss out of the droplet cavity is $\alpha_{leakage}(\lambda)$ and the absorption loss of a thermochromic absorber, is $\alpha_{abs}(\lambda, T)$. If the fluorescent wavelength λ is not at a MDR wavelength, $\alpha_{leakage}(\lambda)$ is large and then lasing condition is not satisfied. In order to verify that florescent-lasing transition shifts to the blue when the absorption loss increases, a non temperature-dependent and non-wavelength-dependent absorber (nigrosin, a black dye) was used (for details see Ref. 1).

Figure 1(a) shows the absorption spectra [$\alpha_{abs}(\lambda, T)$] of the thermochromic absorber, in 85% ISO-propane and 15% water at several liquid temperatures. The $CoC1_2 \bullet 6H_2O$ is the thermochromic absorber. Figure 1(b) shows the usual $\sigma_e(\lambda)$ and $\sigma_a(\lambda)$ of Rhodamine B in ethanol. The Rhodamine B is the lasing dye known to have a large

wavelength separation between the $\sigma_e(\lambda)$ peak and the $\sigma_a(\lambda)$ peak, commonly referred to as having a large Franck-Condon shift. Both the thermochromic absorber and the lasing dye are placed in the liquid droplet, consisting mainly of 85% iso-propanol and 15% water.

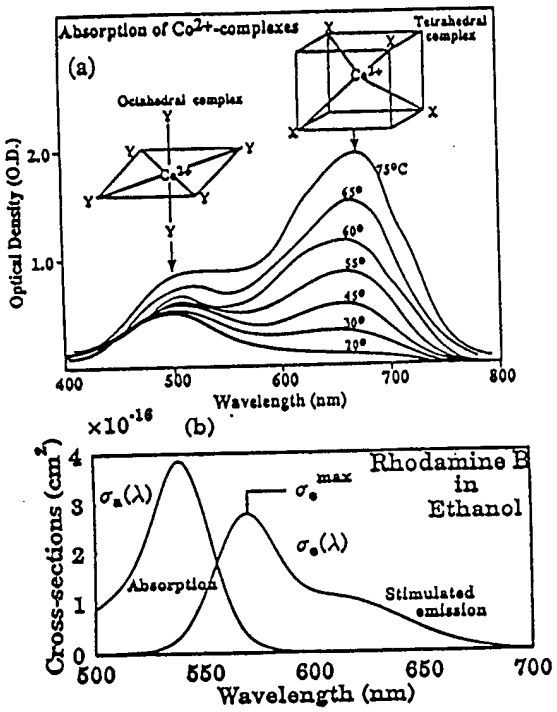

Figure 1

(a) The schematic of the thermochromic absorption spectra of $CoC1_2 \bullet 6H_2O$ in a solution of 85% iso-propanol and 15% water. The inset shows the octahedral and tetrahedral configurations which are responsible for the absorption bands of the Co^{2+} complexes. (b) The absorption $\sigma_a(\lambda)$ and the stimulated emission spectrum $\sigma_a(\lambda)$ of Rhodamine B in ethanol.

The mechanism responsible for the temperature-dependent absorption change in $CoC\ell_2 \bullet 6H_2O$ is known to be related to the temperature-dependent configuration change in the Co^{2+} complexes in the presence of $C\ell^-$ ions and H_2O molecules. In an octahedral configuration of six identical ligands, the electronic transition of Co^{2+} is parity forbidden, because of inversion symmetry associated with the octahedral configuration. In the $CoC\ell_2 \bullet 6H_2O$ solution, the absorption around 500 nm is not completely forbidden, because strict octahedral symmetry is not maintained as the six ligands are not all identical at all times. In a tetrahedral configuration of four identical ligands, the electronic transitions of Co^{2+} is electric dipole allowed. The tetrahedral complex can be mono-, di-, or tri-chloro complexes.

The temperature-dependent configurational change in the complexes can be described by the following type of reactions:

$$Co(H_2O)_6^{2+} + 4C\ell^- + \text{heat} \Leftrightarrow CoC\ell_4^{2-} + 6H_2O \qquad (2)$$

In the $CoC\ell_2 \bullet 6H_2O$ solution, the absorption around 650 nm increases with temperature because there are more tetrahedral configurations formed as the temperature is raised. The addition of heat decreases the octahedral symmetry by increasing the vibration of the ligand molecules and by replacing a few H_2O molecules by iso-propanol. Thereby, the dipole transition and the absorption at 500 nm is more allowed even though there are fewer octahedral sites at increasingly higher temperatures.

Figure 2 shows the lasing and fluorescence spectra of a single droplet as the vibrating orifice temperature ($T_{orifice}$) is changed from 21 °C to 92 °C. The series of peaks in the spectra correspond to the cavity resonances of the droplet. Note that as the $T_{orifice}$ increases, the lasing band shift to the blue. The dye lasing wavelength shifts to the blue because of the increased absorption around 650 nm associated with the thermochromic absorber as the $T_{orifice}$ is raised. Similar blue shift in the lasing spectra of Rhodamine B dye has been observed when we increased concentration and, thereby the absorption of a temperature-independent absorber, nigrosin.

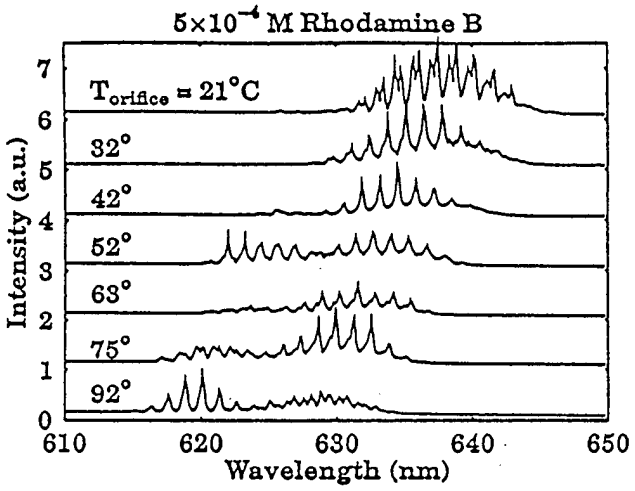

Figure 2

Lasing spectra from microdroplets (with radius ~35 μm) with 5 x 10^{-9} M Rhodamine B in 0.1 M $CoCl_2 \bullet 6H_2O$ solution of 85% iso-propanol and 15% water a $T_{orifice}$ = 21, 32, 42, 52, 63, 75 and 95 °C, respectively. The pump laser power is fixed at ~ 10 MW/cm^2 .

Figure 3 shows the red-end portion of the lasing spectra shown in Fig. 2. The wavelength λ_{trans} marks the intensity transition of lasing (as indicated by a sharp rise) from fluorescence (as shown with a gradual decrease with wavelength). Attempts are being made to deduce the droplet temperature from the temperature dependence of λ_{trans}. (For more details, see Ref. 2).

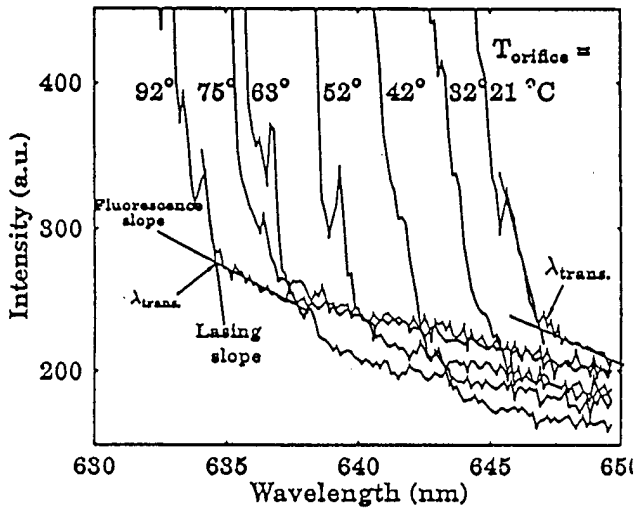

Figure 3

The long wavelength portion of each measured lasing spectrum in Fig. 2 is expanded in order to determine the transition wavelength λ_{trans} between lasing and fluorescence in the microdroplets.

(b) Species Identification through Stimulated Raman Scattering

During the three year AFOSR grant period, another new project was initiated to enhance preferentially the stimulated Raman scattering (SRS) signal from a Raman vibration mode belonging to a minor species within a multicomponent fuel droplet. This technique involved external seeding or injection of light at the Raman-shifted wavelength of the minor species before pumping the droplet with a high-intensity beam. (For more detail, see Refs. 3 - 5).

SRS is Raman amplification of the spontaneous Raman scattering that is generated at the beginning of the radiation-liquid interaction. The amplification can be as much as $\exp(30) \approx 10^{13}$. Hence, SRS is *much more* intense than the well known spontaneous Raman scattering. In an optical cell, SRS is Raman amplification of the spontaneous Raman scattering generated within the entrance face of the cell. Raman amplification occurs for the vibration mode having the largest Raman gain for the i-th species (g_i), which is proportional to the (Raman scattering cross section the i-th species) x (concentration of the i-th species in the multicomponent liquid). In a droplet, the SRS intensity for the i-th species $I_{SRS,i} = I_{spontaneous,i}\, e^{(g_i I_p N 2\pi a)}$, where I_p is the pump intensity, and N is the number of round trips around the droplet circumference. During the photon retention time τ, the photons make N round trips around $2\pi\mathbf{a}$ with the speed of $c/m(\omega)$. The weaker Raman-gain vibration modes never reaches its full intensity, because I_p is depleted while providing gain for the largest Raman-gain g_i vibration mode. In a droplet, the droplet-cavity resonances at different Raman-shifted wavelengths have only partial spatial overlap with the pump and with each other. With less I_p depletion, because of only partial overlap with the droplet-cavity resonances, SRS from the weaker Raman-gain vibration modes can still be amplified. However, the SRS intensity of the minority species is still much lower than that of the majority species.

Without seeding, the SRS builds from spontaneous Raman photons that are generated at the beginning of the laser-material interaction. Should the injected radiation be greater than the spontaneous Raman scattering, the SRS builds initially from a larger number of seeded photons and, hence, can a faster growth rate and achieve a larger final intensity. Two implementation make the external seeding technique viable. First, by using a spectrally broad band seed beam ($\approx$ 2 nm wide), we were able to spectrally discriminate the elastically scattered seed light from the narrow line width SRS, which occurs only on MDR's because at these wavelengths the droplet provides the optical feedback to the SRS process. Second, by incorporating an analyzer in front of the detector that is crossed to the linear polarization of the seed beam, we prevent detector saturation. The elastic scattering by the droplet preserves the polarization of the input beam. Hence the crossed analyzer can block a large fraction of the intense elastically scattered radiation.

Figure 4 illustrates the polarization geometry of the pump, incident seed, elastically scattered seed, and the generated SRS. The seed radiation (at the Raman-shifted wavelength) is horizontally polarized ($\theta = 90°$) and the analyzer is usually vertically polarized ($\theta = 0°$), which blocks out most of the intense elastically scattered radiation. The pump radiation (at the second harmonic of the Nd:YAG laser) can be set at any θ relative to the vertical.

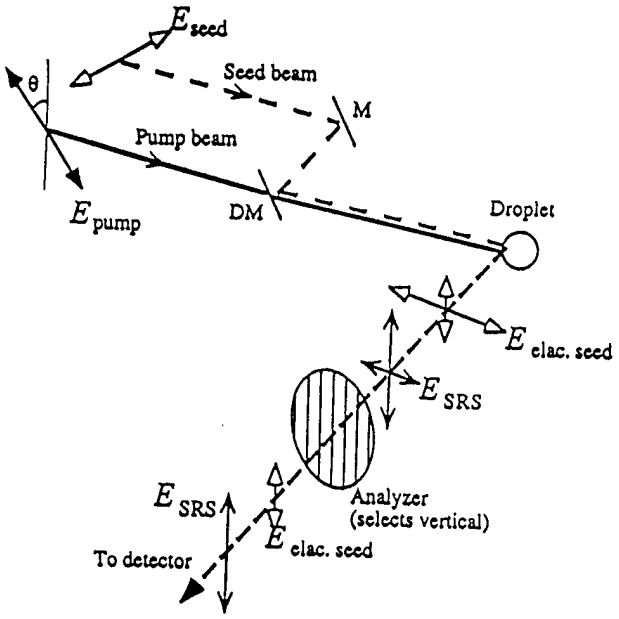

Figure 4. Experimental arrangement for external seeding of SRS. The polarization geometry of the pump, incident seed, elastically scattered seed, and the generated SRS is shown.

Figure 5 shows that by tuning the seed radiation to ≈ 632 nm, the SRS of the weaker gain Raman mode of methanol (at 2944 cm^{-1}), can be made stronger than the SRS of the stronger gain Raman of methanol (at 2835 cm^{-1}). The SRS and the elastically scattering of the seed can be readily distinguished, because the bandwidth of the seed is purposely selected to be much wider than that of the SRS, which acquires the MDR line width as the MDR is providing the optical feedback for the SRS. Note that with seeding at the weaker Raman gain mode, the seeded SRS of the weaker gain mode can be made stronger than the SRS of the stronger gain mode. Whereas without seeding, the SRS of the weaker gain mode is smaller than that of the stronger gain mode.

We have also demonstrated that external seeding of a minority species (3% acetone in water) is feasible. Without seeding at the acetone Raman mode (2925 cm^{-1}), only the SRS of O-H stretching mode of water is detected (3200 and 3400 cm^{-1} bands) [see Fig. 3]. The SRS of 3% acetone is not detected. However, with seeding at the acetone Raman mode, the SRS is definitely observable in Fig. 6. The inset in Fig. 6, shows the SRS with and without seed on a magnified intensity scale.

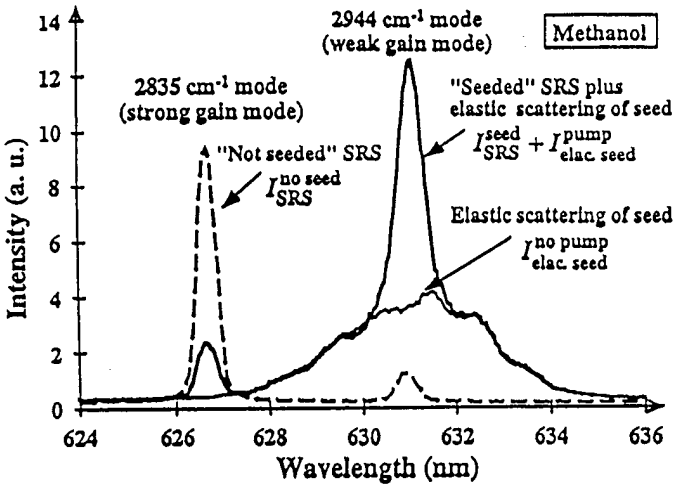

Figure 5. The detected spectra with following conditions: (1) with no pump, only the elastic scattering of the seed is detected; (2) with no seed, only the SRS is detected; and (3) with seed and pump both on, the seeded SRS plus the elastic scattering of the seed are detected. Outside the seed bandwidth, the SRS of the stronger gain mode actually diminishes when the seed beam is on in order to enhance the weaker gain mode.

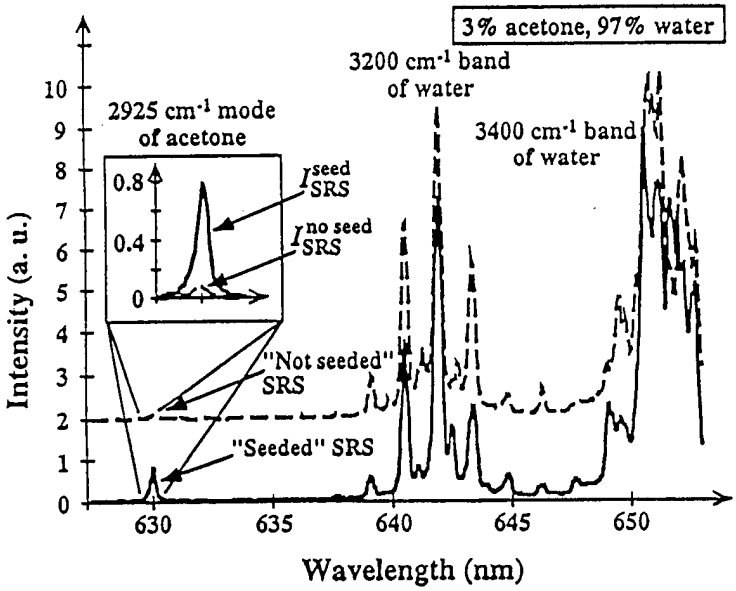

Figure 6. The SRS spectra with and without seed tune to the 3% acetone Raman mode at 2925 cm^{-1}. The elastically scattered spectrum has been subtracted from the seeded SRS spectra.

(c) Injection Seeding and Q-Switching Lasing Droplets

The internal intensity of the SRS (of a strong vibration mode) is more efficient in pumping the SRS (of a weak vibration mode) than the internal intensity of the pump laser (see Ref. 3 and 4). We were motivated to force the droplet lase in a single mode, because the inner intensity of the lasing may serve as a more efficient pump for SRS. Many techniques have been used to force the multimode mode lasers (in our case, the spherical cavity modes) to lase in a single mode. Usually frequency-selective elements are introduced into the cavity. However, for liquid droplets which act as individual lasers, it is not possible to insert a frequency-selective element within the droplet.

We have managed, with injection seeding light a particular wavelength to enhance the intensity from one lasing mode selected among many lasing modes that naturally occur because of the lasing gain profile spans many droplet cavity modes. In fact, competition between the seeded mode and the unseeded lasing modes that have good spatial overlap with the seeded mode prevents lasing on some unseeded lasing modes. Fig. 7 shows that the contrast is increased between one seeded lasing mode and the many unseeded mode. (For details, see Ref. 6). In this injection seeding scheme, the seed pulse precedes the pump pulse by ≈ 2 nsec. The pump pulse duration is 7 - 10 nsec.

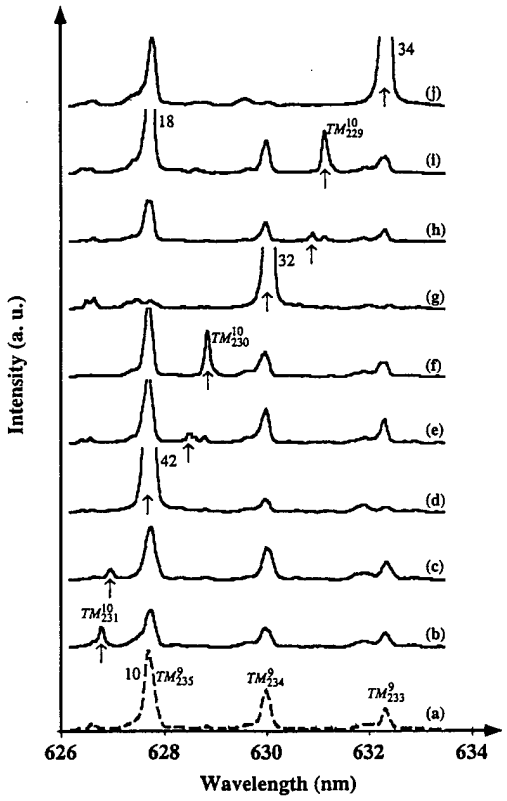

Fig. 7 Lasing spectra from ~21.7-μm dye-doped micro-droplets: (a) not-seeded spectrum, (b) -(j) seeded lasing spectra with the seed wavelength indicated by ↑. All spectra have the same intensity sacale. The intensities of the cutoff peaks are given by the numbers. The modes are identified and labeled TM^{l}_{n}. Each spectrum is a 10-laser shot average. Spectra (f) and (g) show the major effects of seeding.

We were further motivated to increase the intensity of the single mode pulse, above and beyond the gain clamped lasing intensity. In the concluding weeks of the AFOSR grant period, we succeeded in Q-switching a single lasing droplet. Q-switching entails the rapid switching of an optical cavity from a lower Q value to a higher Q value. The unique property of a saturable absorber is that its absorption is higher at low intensity than that at higher intensity. A saturable absorber is usually inserted in the optical Fabry-Perot cavity of a conventional laser. Initially, when the absorption is higher (i.e., the Q is low), lasing is surpressed, even though optical pumping is occurring, Suddenly, when the absorption is switched to a lower amount, lasing can appear with a temporary extra gain that is above the steady-state clamped gain for the cavity with a steady-state higher Q. We attempted to adapt the standard Q-switching approach with saturable absorber in our droplet laser.

To demonstrate that we can indeed decrease the absorption at high input intensity, we measured the elastic scattering spectrum of a droplet (containing a saturable absorber). The broad band input radiation was from a mode-less dye laser amplifier (operating in an amplified spontaneous emission mode). Figure 8 shows that the measured elastic scattering spectrum at the lowest input intensity is commensurate with the predicted elastic

scattering spectrum at the lowest input intensity is commensurate with the predicted elastic scattering spectrum when the droplet has a large imaginary part of the index of refraction (n_i). With higher input intensity, the measured elastic scattering spectrum fits the predicted spectrum with a lower n_i. The elastic scattering experiments demonstrated that we can indeed alter the Q value by varying the intensity of external radiation.

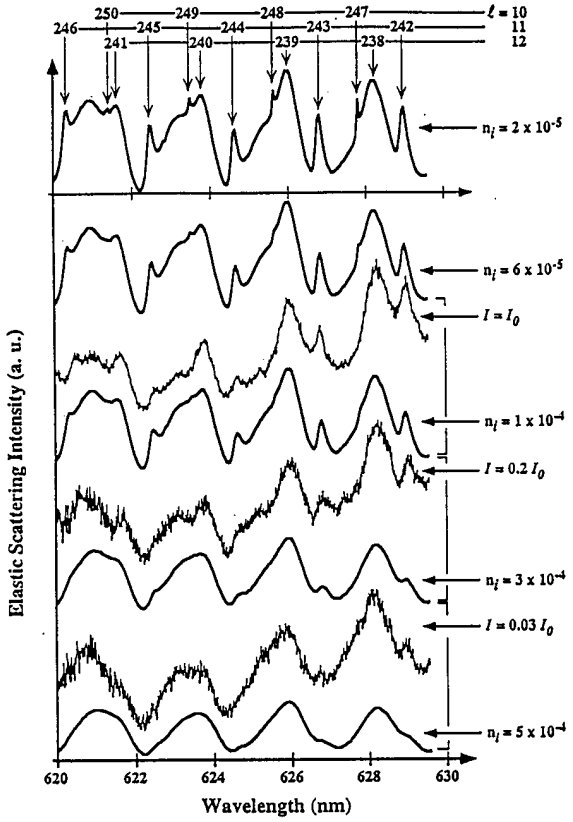

Fig. 8 Elastic scattering spectra of 23.7-μm radius methanol droplets containing 2 x 10^{-4} M DQTCI measured at three different incident intensities I and calculated with five different values for the imaginary part of refractive index n_i. The MDR's are assigned to $TE\,^{10}_{n}$ (n = 247-250), $TE\,^{11}_{n}$ (n = 242-246), and $TE\,^{12}_{n}$ (n = 238-242) modes.

We switched the Q value of the lasing droplets (containing both a lasing dye and a saturable absorber) by illuminating such a droplet with high intensity radiation (refereed to as the bleaching pulse), wavelength selected to at one of the strong-lasing mode. In this Q-switching scheme, the seed pulse follows the pump pulse by ≈ 2 nsec, just opposite to case of injection seeding scheme where the seed pulse precedes the pump pulse by ≈ 2 nsec. Before the bleaching pulse is on, the droplet is weakly lasing (just above threshold), because of the high absorption of the saturable absorber. At steady state conditions, the gain is clamped to the high absorption loss. However, when the bleaching pulse is turned on, the absorption is decreased. For a short time, the original clamped gain exceeds the lowered absorption loss. Furthermore, the bleaching pulse acts as a seeding pulse, stimulating electrons to emit from the upper lasing state to the lower lasing state. For s short time, the gain is higher than the lowered absorption loss. These extra photons, provided by the bleaching pulse, now favors the lasing growth at that selected wavelength which is on a MDR. Consequently, all the net gain (original clamped gain minus the lowered absorption loss) is consumed by amplifying the radiation at the bleaching pulse wavelength. The net result is the generation of a strong single mode (created after the bleaching pulse is on), with the presence of a series of much weaker modes created before the bleaching pulse is on. Whether the dominant lasing mode can efficiently pump the SRS, more so than the pump pulse, remains to be investigated. (See ref. 7 for more details on Q-switching a single lasing droplet).

II. Two- and Three-Dimensional Measurements in Flames

Laser diagnostic techniques have been developed that are capable of two- and three-dimensional mapping of scalars and velocities in turbulent flames. Whenever possible, the techniques are tailored to measure quantities and flow configurations of current interest to combustion modelers. The availability of quantitative data on the spatial and temporal characteristics of structures in turbulent reacting flows will aid in understanding the interaction of chemical reactions with the turbulent motion. A better understanding of this key interaction is important for testing existing models of turbulent combustion as well as for suggesting new models. In the following sections, some of the major accomplishments of the three-year funding period are outlined.

(a) Mixture Fraction Imaging

During the current three-year funding period, significant effort has been put into the development of mixture fraction imaging techniques in turbulent nonpremixed flames. The mixture fraction is defined as the mass fraction of atoms originating in the fuel stream and is independent of the chemical reaction occurring in the flame. The gradient of the mixture fraction is needed to find the scalar dissipation, which determines the rate of molecular mixing in the flow. The mixture fraction and its gradient are important parameters in the modeling of turbulent flames, and the experimental determination of mixture fraction over a wide field is essential for testing these models.

A two-scalar approach for mixture fraction determination was developed by Dr. Sten Stårner and Prof. Robert Bilger at the University of Sydney. Since 1992, we have been collaborating with them to extend the two-scalar approach to imaging experiments. The method assumes unity Lewis number and a simplified one-step reaction between fuel and oxidizer. It has been shown that the measurement of fuel concentration and Rayleigh scattering is sufficient to determine the mixture fraction.

In our mixture fraction imaging experiments, the fuel concentration has been obtained using one of two techniques: (1) laser-induced fluorescence of the fuel or a fuel marker, or (2) Raman scattering from the fuel. The fuel fluorescence work showed early promise due to its high signal strength, but failed due to pyrolysis of the fluorescing species just rich of stoichiometric. The use of Raman scattering to determine the fuel concentration allows the use of simpler hydrocarbons as fuel, resulting in less severe pyrolysis problems (see Ref. 15 and 16).

To maximize the signal/noise of our mixture fraction imaging using the Rayleigh/Raman technique, we have developed a novel intracavity laser imaging configuration. The output coupler from a flashlamp-pumped dye laser is replaced with a cylindrical mirror and the cavity is extended to approximately 2.75 meters. A cylindrical lens is placed within the cavity such that light reflected by the cylindrical mirror is recollimated and fed back into the active medium. The intracavity approach provided a signal 4.2 times larger than that obtained with a conventional extracavity setup (see Ref. 17).

In order to further increase the signal/noise ratio in the Raman data, some degree of smoothing is desirable. Because the Raman and Rayleigh images are highly correlated in the regions where the Raman signal is non-zero, the Rayleigh image can be used to optimize the smoothing of the Raman image. By performing smoothing of the Raman image along constant intensity contours derived from the Rayleigh image, we have shown that it is

possible to increase the signal/noise by a factor of 10, while retaining the gradient information (see Ref. 18).

This experimental setup has been used to investigate a number of different flame configurations, including a lifted methane diffusion flame, a hydrogen fuel diffusion flame, and a piloted nonpremixed methane-air flame (see Ref. 19-21). For this last flame, images were recorded 25 diameters downstream from the 6.1 mm axisymmetric burner. The burner was placed in a 7 m/s filtered coflow to prevent particles from interfering with the Rayleigh data, as well as to reduce soot interference. Flames with nozzle Reynolds numbers ranging from laminar to 34,800, were investigated using air-diluted methane as fuel (30% methane by volume). A sample of the corrected Rayleigh/Raman data, along with temperature and mixture fraction are shown in Fig. 9.

(b) Velocity/Scalar Imaging

A second focus during the current funding period has been the development and application of velocity/scalar imaging. We have performed a series of measurements in a turbulent premixed propane/biacetyl/air flame. In these experiments two separate lasers were used for the PIV and biacetyl fluorescence. The second harmonic of a double-pulsed Nd:YAG laser was used for the PIV measurements. With this laser, the interpulse time could be adjusted continuously from 25-200 μs to enable PIV measurements over a range of flow velocities and spatial resolutions. Biacetyl fluorescence was excited at 440 nm with a flashlamp-pumped dye laser. Both laser beams were overlapped with a dichroic beam splitter and then formed into a single sheet to illuminate a planar region of the flow. The timing of the lasers was arranged so that the dye laser pulse occurred during the period between the two pulses from the Nd:YAG laser.

The flame selected for study was an unsteady premixed propane/biacetyl/air flame, stabilized on a 1.1 cm diameter piloted axisymmetric burner. The average velocity at the burner exit was 4.1 m/s. To enhance the turbulence, a perforated plate with 1 mm diameter holes was placed inside the burner. The air was seeded with both biacetyl vapor and submicron alumina particles and then mixed with propane. Alumina was chosen for particle seeding so that the particles would survive the flame and allow velocity measurements to be performed on both sides of the flame front. The 1.7 cm diameter annular pilot consisted of a premixed propane/air flame that aided in anchoring the main flame to the burner.

For the PIV measurements, Lorenz-Mie scattering from the aerosols was imaged onto a cooled 2048 x 2048 pixel CCD detector oriented normal to the laser sheet. The imaging optics consisted of two camera lenses and an interference filter to block flame luminosity, biacetyl fluorescence, and Lorenz-Mie scattering of the dye laser by seed particles. On the opposite side of the flow, a second cooled CCD detector with an optically-coupled single-stage image intensifier was used to image the biacetyl fluorescence.

In one set of experiments, we concentrated on obtaining measurements with high spatial resolution. (The separation between vectors was 0.165 mm.) With this resolution, the acceleration of the product gases associated with the heat release near the flame front was evident. By using both the scalar and velocity fields, the locations of velocity vectors were identified with either the reactant or the product regions of the flow. The mean reactant and mean product velocity fields were thus obtained from a data set containing 54 independent PIV/PLIF measurements. Instantaneous velocity fluctuations were obtained by subtracting the appropriate mean (reactant or product) velocity from the velocity measured at each point in the flow field. An example of reactant and product velocity fluctuations is shown in Fig. 10 (see Ref. 22).

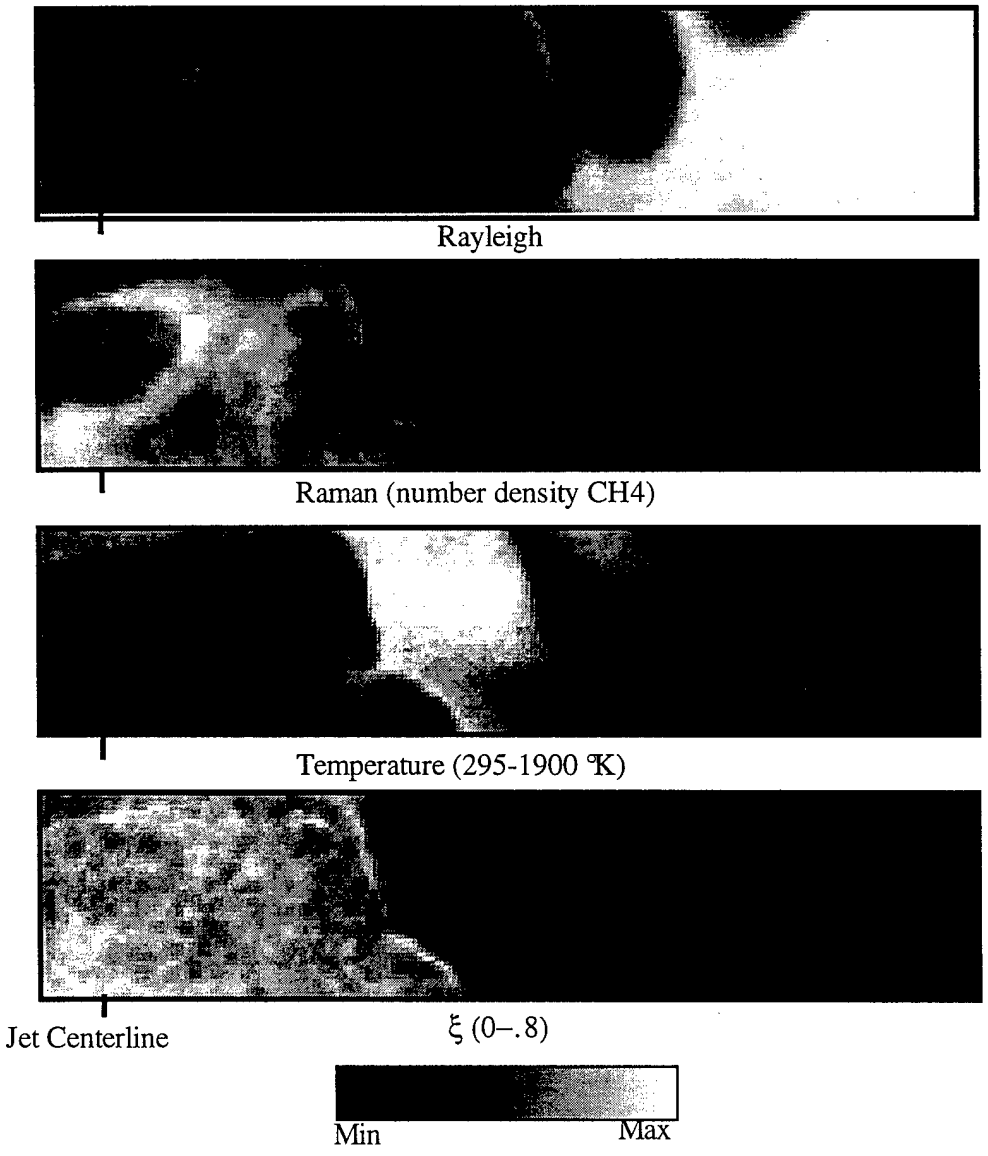

Figure 9. Raman/Rayleigh images from a turbulent nonpremixed flame (Re = 21,300). The measurements were taken 25 diameters downstream (d = 6.1 mm) and cover 6.5 mm in the axial by 30 mm in the radial direction. Also shown are the calculated temperature, and mixture fraction (ξ) for this image pair.

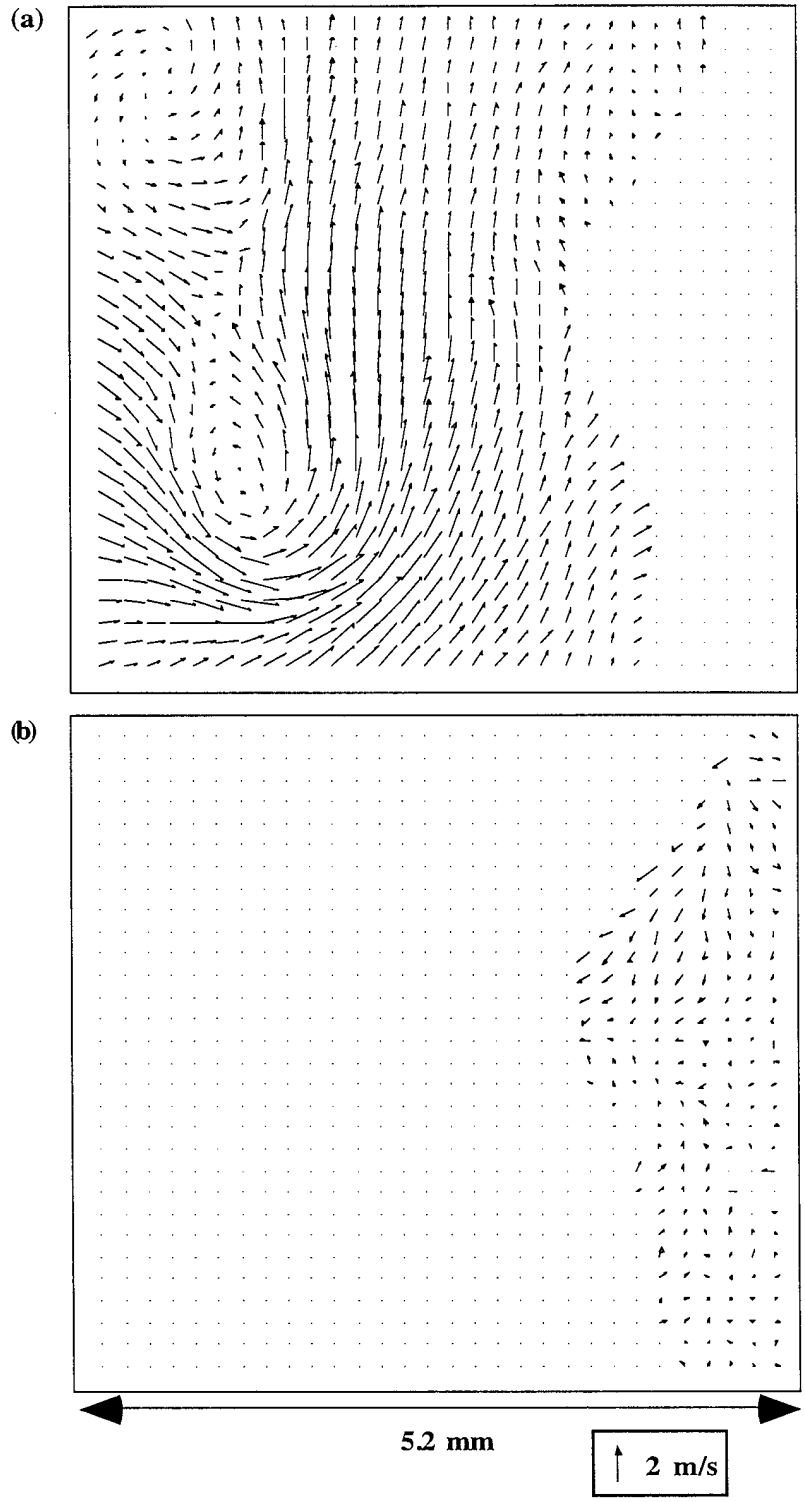

Figure 10. Instantaneous reactant (a) and product (b) velocity fluctuation fields in a turbulent premixed flame. Velocity fluctuations were computed by subtracting the appropriate mean reactant or product velocities from an instantaneous velocity measurement. The scalar image was used in conjunction with the velocity image to identify regions as being either in the reactants or products.

(c) Measurements in Highly Turbulent Premixed Flames

A new set of experiments in highly turbulent premixed flames was initiated within the past year. There is currently a need for quantitative, three-dimensional measurements in premixed flames to assess the applicability of flamelet modeling approaches as well as to advance other modeling techniques such as conditional moment closure (CMC) methods. To be of most use to modelers, the scalar data must be of sufficient quality to allow calculation of three-dimensional gradients (and thus scalar dissipation).

The current experiment involves the simultaneous measurement of Rayleigh scattering from two parallel laser sheets, as well as OH fluorescence from a third laser sheet located between the other two. The laser illumination sheets for the Rayleigh measurements are provided by two separate frequency doubled Nd:YAG lasers, separated temporally by 0.8 μs. The Rayleigh signals were collected by a single camera lens, separated into parts by a 50/50 pellicle beam splitter, and each part was focused onto a separate intensified CCD detector. Cross talk between the Rayleigh signals from the two different sheets was eliminated by gating one intensifier to correspond to the first laser pulse and the second intensifier coincident with the second. Since the accuracy of the cross-sheet component of the gradient is critically dependent on accurate measurement of the separation between sheets, a portion of the laser beams was split off and focused onto a separate unintensified CCD detector. The image from this detector gives a shot-to-shot monitor of the sheet spacing (typically 200 μm) as well as the beam intensity profile.

The OH fluorescence required a third uv laser beam at 283.2 nm corresponding to the $Q_1(7)$ transition of the OH $A^2\Sigma$-$X^2\Pi$ (1,0) system. The OH fluorescence was isolated by an interference filter and imaged onto another intensified CCD detector. The combination of the Rayleigh and OH fluorescence signals in the experiment allowed determination of temperature, progress variable, scalar dissipation, and hydroxyl mass fraction within the imaged region (see Fig. 11).

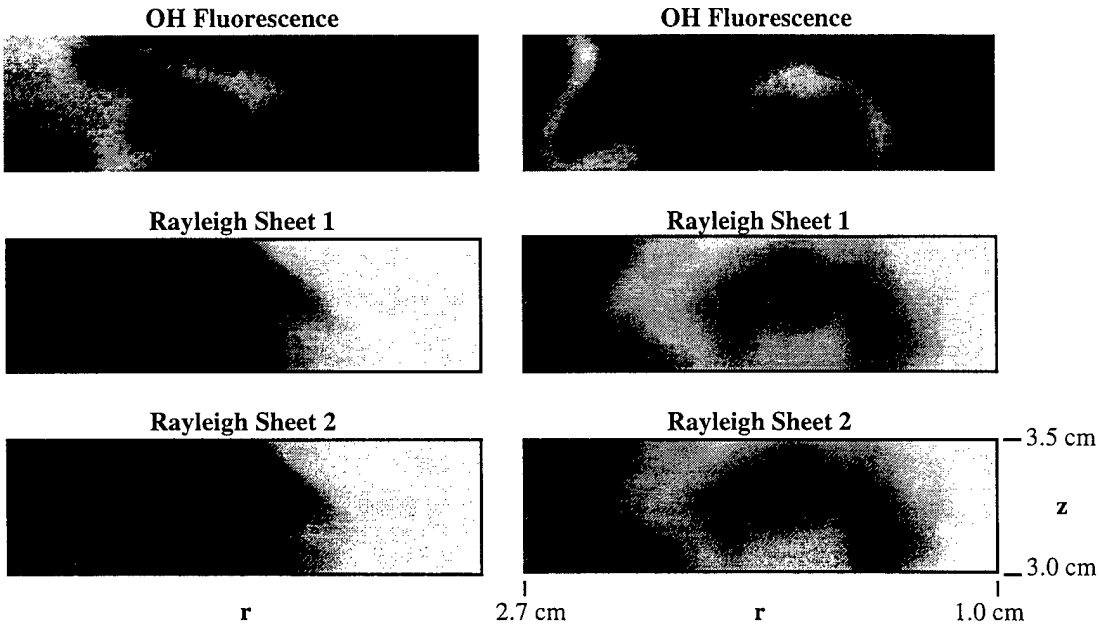

Figure 11. Experimental results obtained from a 38 mm diameter Bunsen flame with an annular pilot. Turbulence was generated by a plate in the approach flow in which 4 mm holes were drilled at 10 mm spacing. The Rayleigh images are used to determine the temperature, progress variable, and scalar dissipation; the OH fluorescence (along with the Rayleigh images) gives the OH mass fraction. The imaged region covers an area of 17 x 5 mm^2, located 30 mm downstream from the burner exit . The equivalence ratio for these shots was $\Phi = 0.6$.

PUBLICATIONS RESULTING FROM THE RESEARCH

I. Nonlinear Spectroscopy of Multicomponent Droplets

1. Janice L. Cheung, Justin M. Hartings and Richard K. Chang, "Different Temporal Behavior for the Forward- and Backward-Circulating Radiation within a Microdroplet," Opt. Lett. 20 1089 (1995).

2. Md. Mohiuddin Mazumder, Gang Chen, Peter J. Kindlmann, R. K. Chang, and James B. Gillespie, "Temperature-Dependent Wavelength Shifts of Dye Lasing in Microdroplets with a Thermochromic Additive," Opt. Lett. 20, 1668 (1995).

3. Md. Mohiuddin Mazumder, Karl Schaschek, Richard K. Chang and James B. Gillespie, "Efficient Pumping of Minority Species Simulated Raman Scattering (SRS) by Majority Species SRS in a Microdroplet of a Binary Mixture," Chem. Phys. Lett., 239, 361 (1995).

4. Md. Mohiuddin Mazumder, Mitchell H. Fields, Justin M. Hartings, Xiaoyun Pu, Alfred S. Kwok, Karl Schaschek and Richard K. Chang, "Enhancing Stimulated Raman Scattering of Weaker Gain Raman Modes in Microdroplets by Seeding and Efficient Pumping," in Nonlinear Frequency Generation and Conversion, SPIE Proceedings Series, 27, 352 (1996).

5. Mitchell H. Fields, Jürgen Popp, and Richard K. Chang, "External Seeding of Stimulated Raman Scattering in Microdroplets," Opt. Lett. 21, 1457 (1996).

6. Jürgen Popp, Mitchell H. Fields, Richard K. Chang, "Injection Seeding of Lasing in Microdroplets," Opt. Lett 22, 139 (1997).

7. Jürgen Popp, Mitchell H. Fields, and Richard K. Chang, "Q-Switching by Saturable Absorption in Microdroplets: Elastic Scattering and Laser Emission," submitted to Optics Letters (1997).

8. J. Christian Swindal, G. Chen, A. Serpengüzel, R. K. Chang, and W. P. Acker, "Spray Diagnostics with Lasing and Stimulated Raman Scattering," Progress in Astronautics and Aeronautics, Vol. 171, "Recent Advances in Spray Combustion: Spray Combustion Measurements and Model Simulation", Vol. II, edited by K. K. Kuo, (American Institute of Aeronautics and Astronautics, Washington, DC 1996), p 63.

9. Gang Chen, Md. Mohiuddin Mazumder, J. Christian Swindal, Karl Schaschek, and Richard K. Chang, "Nonlinear Optical Emission and Scattering in Micrometer-sized Droplets," in Proceedings of the AGARD Symposium on High Power Microwaves (HPM), Ottawa, Canada, May 2-5, 1994, AGARD CP-564 (NATO, Neuilly Sur Sein, France 1995, p. 24-1.

10. Richard K. Chang, Gang Chen and Md. Mohiuddin Mazumder, "Nonlinear Optics in Micro-Meter Sized Droplets," in Proceedings of the NATO ASI series E, 314, 75 - 99, edited by M. Ducloy and D. Bloch (Les Houches France, 1995), Kluwer Academic Publishers, The Netherlands, 1996.

11. Gang Chen, Md. Mohiuddin Mazumder, Richard K. Chang, J. Christian Swindal and William P. Acker, "Laser Diagnostics for Droplet Characterization," Progress in Energy & Combustion Science 22, 163 (1006).

12. J. L. Cheung, J. M. Hartings, and R. K. Chang, "Nonlinear Optics of Microdroplets Illuminated by Picosecond Laser Pulses," in Handbook of Optical Properties, Vol.II, *Optics of Small Particles, Interfaces and Surfaces* , CRC Press, 1996.

13. Md. Mohiuddin Mazumder, Dipakbin Q. Chowdhury, Steven C. Hill, and Richard K. Chang, "Optical Resonances of a Spherical Dielectric Microcavity: Effects of Perturbations," in Optical Processes in Microcavities, edited by Richard K. Chang and Anthony J. Campillo, (World Scientific Publishers), p 209 1996.

14. J. Christian Swindal, Gang Chen, Karl Schaschek, and Richard K. Chang, "Measurement of the Evaporation Rates of Closely Spaced Flowing Droplets by Optical Cavity Resonances," Journal of Atomization and Sprays, 6, 331 (1996).

II. Two- and Three-Dimensional Measurements in Flames

15. J.H. Frank, K.M. Lyons, D.F. Marran, M.B. Long, S.H. Stårner, and R.W. Bilger, "Mixture Fraction Imaging in Turbulent Nonpremixed Hydrocarbon Flames," *Proceedings of the Twenty-Fifth Symposium (International) on Combustion*, (The Combustion Institute, Pittsburgh, 1994), p. 1159.

16. S.H. Stårner, R.W. Bilger, K.M. Lyons, J.H. Frank, and M.B. Long, "Conserved Scalar Measurements in Turbulent Diffusion Flames by a Raman and Rayleigh Ribbon Imaging Method," *Combust. Flame* **99**, 347 (1994).

17. D.F. Marran, J.H. Frank, M.B. Long, S.H. Stårner, and R.W. Bilger, "An Intracavity Technique for Improved Raman/Rayleigh Imaging in Flames," *Opt. Lett.* **20**, 791 (1995).

18. S.H. Stårner, R.W. Bilger, and M.B. Long, "A Method for Contour-Aligned Smoothing of Joint 2D Scalar Images in Turbulent Flames," *Combust. Sci. Tech.* **107**, 195 (1995).

19. S.H. Stårner, R.W. Bilger, J.H. Frank, D.F. Marran, and M.B. Long, "Mixture Fraction Imaging in a Lifted Methane Jet Flame," *Combust. Flame* **107**, 307 (1996).

20. S.H. Stårner, R.W. Bilger, J.H. Frank, D.F. Marran, and M.B. Long, "Measurements of Mixture Fraction and Scalar Dissipation in a Turbulent Hydrogen Diffusion Flame," paper presented at the 15th International Colloquium on the Dynamics of Explosions and Reactive Systems, University of Colorado, Boulder, CO, July 30 - August 4 (1995).

21. S.H. Stårner, R.W. Bilger, M.B. Long, J.H. Frank, and D.F. Marran, "Scalar Dissipation Measurements in Turbulent Jet Diffusion Flames of Air Diluted Methane and Hydrogen" submitted to *Combust. Sci. Tech.*

22. J.H. Frank, K.M. Lyons, and M.B. Long, "Simultaneous Scalar/Velocity Field Measurements in Turbulent Gas-Phase Flows," *Combust. Flame* **107**, 1, (1996).

SCIENTIFIC COLLABORATORS

In addition to the Co-Principal Investigators, the following people have participated in this project:

I. Nonlinear Spectroscopy of Multicomponent Droplets

Outside Scientists:	William P. Acker (Texaco) Dipakbin Q. Chowdhury (Corning) James B. Gillespie (Army Research Lab.) Steven C. Hill (Army Research Lab.) Thomas Jackson (Air Force Aero-Propulsion Lab.) Ali Serpengüzel (Bilkent University, Turkey) J. Christian Swindal (Texaco) Kenneth Young (Chinese Univ. of Hong Kong)
Colleague:	Peter J. Kindlmann (Yale Univ.)
Post Doctoral Scientist:	Gang Chen Jürgen Popp Karl, Schaschek
Graduate Students:	Janice L. Cheung Mitchell H. Fields Justin M. Hartings Md. Mohiuddin Mazumder

II. Two- and Three-Dimensional Measurements in Flames

Outside Scientists:	Sten Stårner (U. of Sydney) Robert Bilger (U. of Sydney) William P. Acker (Texaco)
Graduate Students:	Jonathan Frank Kevin Lyons David Marran Ping Lin

LECTURES PRESENTED ABOUT THE RESEARCH

Richard K. Chang:

"Nonlinear Spectroscopy Of Multicomponent Droplets", AFOSR Contractors Meeting, Virginia Beach, 6/3-7/96.

"Nonlinear Optical Interactions in Microdroplets: Possible Applications?" Northwestern University, 5/16/96.

"Optical Diagnostics of Droplets: Temperature and Physical and Chemical Properties" Caltech, Pasadena, CA, 5/10/96.

"Physics and Applications of Microcavities", Corning, Inc., Corning, NY, 10/20/95.

"Optical Diagnostics of Droplets," Gordon Conference, Plymouth, New Hampshire, 7/10/95.

"Lasing Spectral Shifts Caused by Perturbations in Microdroplets", ICONO/LO '95 Conference, St. Petersburg, Russia, 6/26/95.

"Nonlinear Optics in Micro-Meter Sized Droplets, NATO Advanced Study Institute Conference on Quantum Optics of Confined Systems, Les Houches, France, May 23 - June 2, 1995, (two lectures).

"Nonlinear Spectroscopy of Multicomponent Droplets" Physics Department, New Mexico State University, Las Cruces, NM, November 16, 1994.

"What can we learn about the Physical and Chemical Properties of Droplets from Nonlinear Spectroscopy?" Physics Dept., Worcester Polytechnic Institute, Worcester, MA, November 7, 1994.

"Determination of Flowing Droplet Properties from Stimulated Light Emission" Chemical Engineering Department, University of Maryland, College Park, MD, September 13, 1994.

"Determination of Flowing Droplet Properties from Stimulated Light Emission," 12th U.S. National Congress of Applied Mechanics, Seattle, WA, June 26, 1994.

"Nonlinear Spectroscopy of Multicomponent Droplets," AFOSR Contractors Meeting in Propulsion, North Lake Tahoe, NV, June 8, 1994.

"Nonlinear Optical Effects in Aerosols," Battlefield Environment Directorate, White Sands Missile Range, NM, May 10, 1994.

"Nonlinear Optical Emission and Scattering in Micrometer-Sized Droplets," AGARD Symposium on High Power Microwaves (HPM), Ottawa, Canada, May 4, 1994.

"Lasing Droplets: Size and Shape Determination," Physics Department, Lehigh University, Bethlehem, PA, April 7, 1994.

"Determination of Flowing Droplet Properties from Stimulated Light Emission," International Aerosol Symposium, Karpov Institute, Moscow, Russia, March 21-25, 1994.

Marshall B. Long

"Laser Diagnostics Advances in Premixed and Non-Premixed Flames," Mechanical Engineering Seminar, Cambridge University, Cambridge, England, April 14, 1994.

"Multi-Parameter Imaging Diagnostics of Reacting and Non-Reacting Flows," Twelfth U.S. National Congress of Applied Mechanics, Seattle, WA, June 26 - July 1, 1994. (invited)

"Imaging and Image Processing," Imaging Techniques for Combustion and Flow, Cranfield University, UK, February 15, 1995. (Keynote Speaker)

"Multi-Parameter Imaging Diagnostics of Reacting and Non-Reacting Flows," Seminar Series on Measurements of Fluid Fields, Ohio State University, April 4, 1995.

"Two- and Three-Dimensional Measurements in Flames," AFOSR Contractor's Meeting in Airbreathing Combustion, University of Michigan, June 13, 1995.

"Experimental and Computational Study of Nitric Oxide in an Axisymmetric Laminar Diffusion Flame," Sydney University Department of Mechanical Engineering, Sydney, Australia, March 8, 1996.

"Mixture Fraction Imaging in Turbulent Nonpremixed Flames," Department of Mechanical Engineering, Yale University, New Haven, CT, September 18, 1996.

"Mixture Fraction Imaging in Turbulent Nonpremixed Flames," Department of Mechanical and Aerospace Engineering, Princeton University, Princeton, NJ, September 24, 1996.

"Experimental and Computational Study of Laminar Diffusion Flames in a Microgravity Environment," NASA Scientific and Technical Advisory Council Symposium, Moscow, Russia, November 20, 1996.

INTERACTIONS WITH OTHER LABORATORIES

Richard K. Chang:

Air Force Aero-Propulsion Laboratory, Fuel and Lubrication Division, WRDC/POSF, Wright Patterson Air Force Base, Ohio
Dr. Mel Roquemore and Dr. Thomas Jackson

Texaco Research Labs, Beacon, NY
Dr. William Acker

U.S. Air Force, Armstrong Laboratory, Edgewood Research Development and Engineering Center, Aberdeen Proving Ground, MD
Dr. Steven C. Hill (now at ARL, Adelphil, MD)

Marshall B. Long:

University of Sydney, Sydney, Australia
Dr. Sten Stårner and Professor Robert W. Bilger

Texaco Research Labs, Beacon, NY
Dr. William Acker

Imperial College of Science and Technology, London, England
Dr. P. Lindstedt

DEGREES AWARDED

Janice L. Cheung, Ph.D., May 1995 (Advisor, R.K. Chang)

Mitchell H. Fields, Ph.D., May 1997 (Advisor, R.K. Chang)

Justin M. Hartings, Ph.D., May 1997 (Advisor, R.K. Chang)

Md. Mohiuddin Mazumder, Ph.D. May 1996 (Advisor, R.K. Chang)

Jonathan Frank, Ph.D., May 1995. (Advisor, M. B. Long)

Kevin M. Lyons, Ph.D., May 1994. (Advisor, M. B. Long)

David Marran, Ph.D., May 1997. (Advisor, M. B. Long)